Nuclear Engineering and Technology 55 (2023) 3591–3598

Contents lists available at ScienceDirect

Nuclear Engineering and Technology

journal homepage: www.elsevier.com/locate/net

Original Article

Measurement of undesirable neutron spectrum in a 120 MeV linac

Yihong Yan [a], Xinjian Tan [b], Xiufeng Weng [b], Xiaodong Zhang [b], Zhikai Zhang [c], Weiqiang Sun [a], Guang Hu [a, **], Huasi Hu [a, *]

[a] School of Nuclear Science and Technology, Xi'an Jiaotong University, Xi'an, 710049, China
[b] State Key Laboratory of Intense Plused Radiation Simulation and Effect, Northwest Institute of Nuclear Technology, Xi'an, 710024, China
[c] School of Applied Physics, Xi'an Jiaotong University, Xi'an, 710049, China

ARTICLE INFO

Article history:
Received 25 February 2023
Received in revised form
11 May 2023
Accepted 13 June 2023
Available online 19 July 2023

Keywords:
Neutron spectrum
Undesirable neutrons
Linac
Bonner sphere spectrometer

ABSTRACT

Photoneutron background spectroscopy observations at linac are essential for directing accelerator shielding and subtracting background signals. Therefore, we constructed a Bonner Sphere Spectrometer (BSS) system based on an array of BF_3 gas proportional counter tubes. Initially, the response of the BSS system was simulated using the MCNP5 code. Next, the response of the system was calibrated by using neutrons with energies of 2.86 MeV and 14.84 MeV. Then, the system was employed to measure the spectrum of the ^{241}Am–Be neutron source, and the results were unfolded by using the Gravel and EM algorithms. Using the validated system, the undesirable neutron spectrum of the 120 MeV electron linac was finally measured and acquired. In addition, it is demonstrated that the equivalent undesirable neutron dose at a distance of 3.2 m from the linac is 19.7 μSv/h. The results measured by the above methods could provide guidance for linac-related research.

1. Introduction

The neutron background spectrum is important for designing the shielding of an electron linear accelerator (linac), the radiation protection protocols, and making the background corrections. Since the completion of the Xi'an 120 MeV electron linac [1], many related application experiments have been carried out based on it, such as cross-section measurement [2], fast neutron resonance transmission analysis (FNRTA) [3], crystal luminescence properties analysis [4], single event effect [5,6] and other experimental studies. However, in the research process, it was found that when power was applied to the accelerator, due to field emission, the electrons were accelerated in the accelerating tube and produced a bremsstrahlung effect with the accelerating tube or surrounding materials, and then photoneutrons were generated by X-rays in (X, n) reactions. Around linear accelerators, where electrons are accelerated and reach their maximum energy, electrons collide with a high-Z target to produce direct (characteristic) and bremsstrahlung (continuously distributed) X-rays that induce (X, n) reactions. Additionally, neutrons are produced by electrons in (e, e'n) or (e, n) nuclear reactions [7,8]. The neutrons became an undesirable part of the accelerator and affected the correctness of the measurement results in the experiments. In the measurement of neutron cross-sections [2], for instance, photoneutrons will increase the measurement uncertainty, and in scintillator performance analysis experiments [4], photoneutrons are considered the background to influence the measurement of the scintillator luminescence process. This component of the photoneutrons as the accelerator backdrop will have an effect on the measurement work described in Refs. [2–6] and the subsequent experimental work. At the same time, there are few studies on the influence of this part of the neutrons, and the specific influence of this part of the undesirable neutrons on the experimental data cannot be known. Therefore, in order to carry out effective background shielding for the physical system in the accelerator application experiment and remove the influence of the background signal, it is necessary to figure out the characteristics of the operating undesirable neutrons and to conduct their energy spectrum and intensity measurements.

The measurement of the neutron spectrum has been refined for a considerable amount of time, such as the measurement of the neutron spectrum by activation foils [9,10], the measurement of fast neutrons by liquid scintillators [11,12], the measurement of fast neutrons by proportional counters with moderators [13–17], and the measurement of the neutron spectrum by the BSS that uses a

* Corresponding author.
** Corresponding author.
E-mail addresses: guanghu@mail.xjtu.edu.cn (G. Hu), huasi_hu@mail.xjtu.edu.cn (H. Hu).

https://doi.org/10.1016/j.net.2023.06.023

gold activation foil as a thermal neutron detector [18], etc. The X-ray fluence produced in the linear accelerator is orders of magnitude larger than the neutron fluence. The radiation field is mixed (neutrons and photons), intense, and pulsed. Radiation measurements with active detectors have the problem of longer dead times and pulse pileup. In order to overcome these drawbacks, a neutron detector having low sensitivity to X-rays and greater efficiency to detect neutrons must be selected. The Bonner sphere spectrometer with moderator added has the advantages of high neutron sensitivity, low γ-ray sensitivity, and isotropic response [19–23]. As a result, the Bonner sphere spectrometer was chosen as the detector for measuring the neutron spectrum in the experiment. Despite the fact that X-rays deposited less energy in the sensitive area during the experiment, the high intensity of X-rays caused the stacking of measurement signals, which led to inaccurate measurement results. In order to ensure that the X-rays deposited in the multichannel middle and low channel regions could be separated from neutrons, we lowered the voltage of the accelerating tube during the experiment. The X-rays were then deducted as the test background. Due to the escalating price of ^{3}He gas around the world, more and more neutron detectors are opting for BF_3 gas, which has a low price and a high detection response to slow and thermal neutrons. Therefore, we chose BF_3 as the sensitive element of the proportional counter to detect neutrons.

In this study, a ten-sphere BSS system was assembled by using BF_3 proportional counter tubes as detectors, and the tubes were wrapped with or without polyethylene spherical shells of different thicknesses. By simulating, calculating, and calibrating the energy response of the BSS system, and using the system to measure the spectrum of the ^{241}Am–Be neutron source, we evaluated the reliability and accuracy of the system in measuring the fast neutron spectrum. Finally, we employed the system and, for the first time, measured the neutron spectrum when the Xi'an 120 MeV electron linac was applied with power.

2. Methods and materials

Through simulation and calibration of the detection response of the BSS system, the actual detection response was obtained. The system was also used to measure the spectrum of the ^{241}Am–Be neutron source for the verification experiment. Then, the verified system was applied to the measurement of the undesirable neutron spectrum of the linac with power applied. The measurement results can be used to conduct effective neutron background shielding for physical systems in other experiments and, at the same time, to provide guidance for radiation protection and other related work. Fig. 1 is the BSS system test flow chart.

2.1. The BSS system response calculation and calibration

The BSS system consists of 10 polyethylene spheres and a centrally placed BF_3 proportional counter tube. However, due to limited conditions, we only used one BF_3 detector for multiple measurements in subsequent calibration experiments and neutron spectrum measurements. The central spherical tube makes the detection response of the BSS isotropic. In the experiment, neutrons with different energies were moderated into thermal neutrons after passing through the polyethylene spherical shells of different thicknesses and reacting with ^{10}B (n, α) in the sensitive volume of the detectors. Under the action of the electric field, the ^{7}Li and α particles produced by the nuclear reactions ionized in the sensitive volume to generate a large number of positive and negative ion pairs, thereby sending signals to the collector. By recording the signals, the nuclear reactions were counted. The BF_3 spherical gas detectors produced by Beijing Nuclear Instrument Factory were selected after investigation. The diameter of the spherical tube is 54 mm, the pressure inside the tube is 0.66 atm, and the plateau is 1600–1900 V. Its structure is shown in Fig. 2, and the numbers noted in the figure are also explained below the figure.

To obtain the neutron spectrum in the required energy range, the polyethylene spherical shell thicknesses of the BSS need to be selected. The neutrons of different energies are moderated by the shells of different thicknesses, so as to realize the wide-range measurement of the system in the detected energy range. Through research and calculation, polyethylene spherical shells with diameters of 0 cm (without polyethylene spherical shell), 9.78 cm, 11.75 cm, 14.29 cm, 17.31 cm, 20.91 cm, 24.97 cm, 26.25 cm, 30.25 cm, and 38.05 cm were selected as moderators to construct the system to measure the neutron spectrum [24–26]. Before the experiment, the MCNP5 code [27] and the ENDF/B-VII [28] were used to simulate and calculate the detection response of the system. During the simulation, the F4 card and the FM card were used to count the nuclear reactions that occurred under specific reaction conditions in the sensitive volume. We simulated the ^{10}B(n,α)^{7}Li reaction using the FM card in the Bonner sphere with reaction ID 107. The S(α,β) treatment is included in the calculations. This treatment takes into account the impact of polyethylene's chemical bonding and crystalline structure on thermal neutron scattering [18,29,30].

During the simulation process, MCNP was used to model the above-mentioned detectors. The model is shown in Fig. 3 below. In this figure, the detector is located in the center of the sphere, and BF_3 gas at a pressure of 0.66 atm filled the interior of the stainless steel shell. The modeling procedure utilized a flat source, and the neutron beam was a parallel beam hitting the sphere's surface. Each time, a total of 10^{7} particles were emitted. The uncertainty of a single simulation was guaranteed to be less than one percent, and the findings could be trusted.

The material settings of the simulation process are shown in Table 1.

The detection response of the Bonner sphere i is defined as the ratio of the neutron counts N detected in the sensitive volume to the neutron fluence rate of energy E_j [18], as shown in Eqn. (1) [31]:

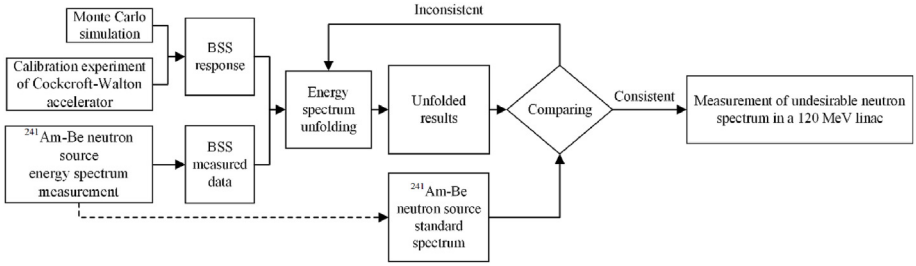

Fig. 1. BSS system test flow chart.

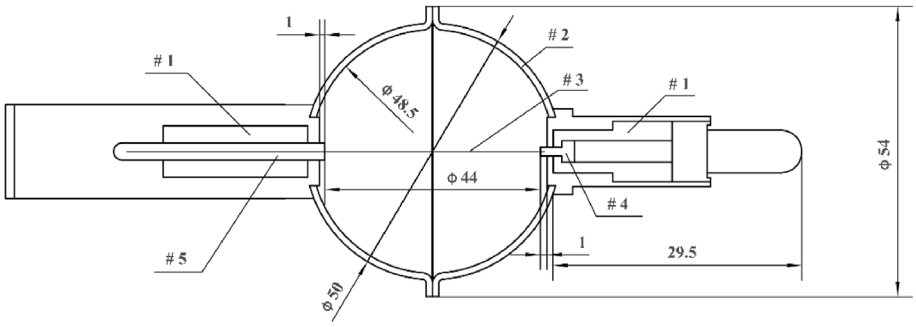

Fig. 2. Structure diagram of the BF_3 proportional counter tube.

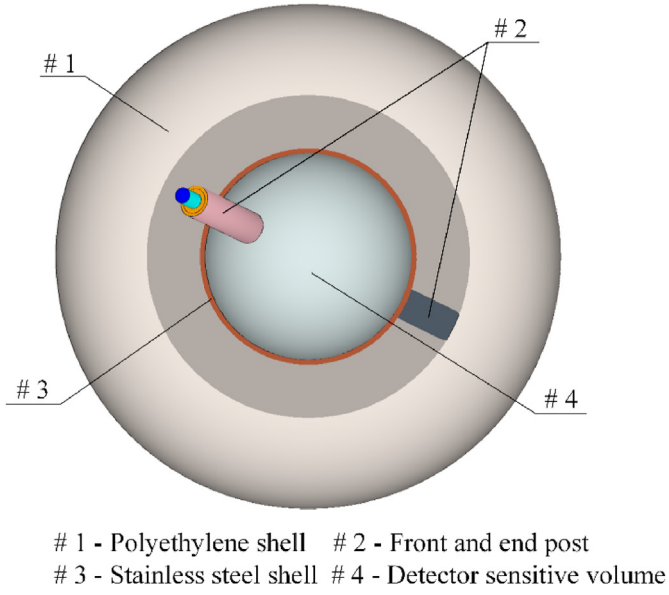

Fig. 3. Schematic diagram of the MCNP5 simulation structure.

Table 1
MCNP5 simulation settings.

Simulation setting	Type
BF_3 gas pressure	0.66 atm
^{10}B:^{11}B ratio	1:4
Polyethylene density	0.95 g/cm^3
Stainless steel density	7.92 g/cm^3
Al_2O_3 ceramic	3.70 g/cm^3

$$R_{ij} = \frac{N}{\Phi_j} \tag{1}$$

The detection response obtained from this is a relative value, and the detection response of the system needs to be calibrated before the spectrum is measured. The calibration experiment was carried out at the Cockcroft-Walton accelerator of the China Institute of Atomic Energy. The Cockcroft-Walton accelerator accelerates the deuterium ions to bombard the solid deuterium target and tritium target, and the D-D and D-T reactions occur, respectively, to produce 2.45 MeV and 14.1 MeV neutrons. It is outstanding with its high neutron yield, close-to-point-source beam spot shape, and satisfactory mono-energetic neutron beam. Moreover, its inclined channel hall (33° to the beam direction) has less gamma background and less influence from neutron scattering, so the calibration experiment was conducted in the hall.

Prior to the calibration experiment, the neutron energy at the inclined channel was determined using the Q equation. The Cockcroft-Walton accelerator's incidence deuterium ion energy is 150 keV, and the Q equation is shown below:

$$Q = \left(\frac{M_b}{M_B} + 1\right)E_b + \left(\frac{M_a}{M_B} - 1\right)E_a - \frac{2\sqrt{E_a E_b M_a M_b}}{M_B}\cos\theta_l \tag{2}$$

where Q is the reaction energy (MeV), M_b is the mass of neutron (u), M_B is the mass of ^{3}He or ^{4}He (u), M_a is the mass of deuterium (u), E_a is the energy of deuterium (MeV), E_b is the energy of neutron (MeV), and θ_l is the angle of deflection.

After calculation, it can be seen that the neutron energy produced by the D-D and D-T reactions in the inclined channel hall is 2.86 MeV and 14.84 MeV, respectively. Due to the limitations of experimental conditions, the calibration was only conducted based on a limited number of Bonner spheres. The experimental calibration layout is shown in Fig. 4. The left side of the figure shows the direction of the deuterium ion beam. The deuterium ions produce neutrons after D-D and D-T reactions with the target on the inclined pipe. The spectrometer system in the inclined pipe hall can be calibrated through the collimation hole.

The detector and the beam exit were centered by the laser, and the position at which the largest diameter detector could be completely covered by neutrons was determined by calculation. Due to the different sizes of spheres, centering was required for experiments on Bonner spheres with different diameters. During the experiment, a voltage of 1800 V was applied to the detector through a high-voltage power supply, ±24 V was applied to the preamplifier through a DC power supply. Both supplies were regulated by UPS. The main amplifier and the multi-channel pulse amplitude analyzer used 572 and 927 plug-ins made by ORTEC, respectively. The MAESTRO software was used with the multi-channel pulse amplitude analyzer to count nuclear reactions on the computer.

The neutron flux on the BSS was obtained by the associated particle method. The particle measurements were obtained by the State Key Laboratory of the China Institute of Atomic Energy. The detector used in the measurement is a GM8IRA(NA) detector which is a semiconductor detector (silicon) with a volume of 8 mm, a low resistivity of 200~500 Ω/cm, and a bias voltage of 5–20 V. This

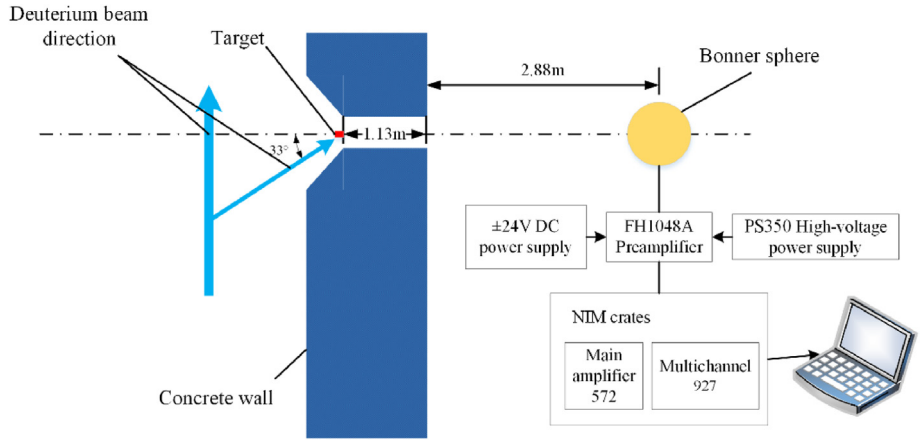

Fig. 4. Experimental site layout.

smaller detector was chosen because its background count is proportional to the detector volume, and it has a low stopping power, which can easily separate protons from α particles. Then, the neutron flux on the BSS surface can be obtained by using the following equation:

$$\Phi = \frac{k\Omega N_a}{S} \tag{3}$$

where Φ is the neutron flux density ($cm^{-2}\bullet s^{-1}$), k is the conversion coefficient of the α particle and neutron flux density given by the laboratory, Ω is the solid angle of the Bonner sphere (sr), N_a is the α particle count rate (s^{-1}), and S is the cross-sectional area of the Bonner sphere (cm^2). According to the statistics published by the China Institute of Atomic Energy, the conversion coefficients k of the D-D and D-T neutron sources are 1.135×10^6 and 1.003×10^6, respectively. The BSS count was measured simultaneously with neutron flux, and the detection response of the BSS system was then calibrated by Eqn. (1) to Eqn. (3).

2.2. Unfolding algorithms

Since the number of BSS spheres is far less than the number of energy points required to measure the spectrum, an algorithm is needed to unfold the spectrum of this undetermined equation to find the best solution. The principle of the algorithm is shown in Eqn. (4):

$$N_i = \int_0^\infty R_i(E)\Phi(E)dE \quad (i = 1, 2, \cdots, n) \tag{4}$$

where N_i is the count rate recorded by the Bonner sphere i (s^{-1}), i is no more than n, $R_i(E)$ is the energy response of detector i to neutrons with energy E (cm^2), and $\Phi(E)$ is the flux density of neutrons with energy E ($cm^{-2}\bullet s^{-1}$).

Eqn. (4) is an undetermined equation that needs to be unfolded using the algorithm. There are many unfolding algorithms for solving underdetermined equations, such as unfolding programs based on the least-square method, maximum entropy and Bayesian theory, the genetic algorithm, and the neural network algorithm. After research, Gravel and EM algorithms were selected to unfold the neutron spectrum.

Gravel is an iterative algorithm that evolved from the SAND-II algorithm. It was initially proposed by the PTB, i.e., the German National Metrology Institute, for solving the pulse amplitude spectrum of the particles, and the iterative equation is as follows [32]:

$$\Phi_j^{K+1} = \Phi_j^K \, exp\left(\frac{\sum_i W_{ij}^K \, ln\left(\frac{N_i}{\sum_{j'} R_{ij'}\Phi_{j'}^K}\right)}{\sum_i W_{ij}^K}\right) \tag{5}$$

$$W_{ij}^K = \frac{R_{ij}\Phi_j^K}{\sum_{j'} R_{ij'}\Phi_{j'}^K} \times \frac{N_i^2}{\sigma_i^2} \tag{6}$$

where Φ_j^{K+1} is the flux density of j energy neutrons in the K+1 iteration ($cm^{-2}\bullet s^{-1}$), Φ_j^K is the flux density of j energy neutrons in the K iteration ($cm^{-2}\bullet s^{-1}$), W_{ij}^K is the weighting factor under j neutron energy at sphere i, N_i is the count rate recorded by the Bonner sphere i (s^{-1}), and σ_i is the measurement error characterizing the measured value N_i when sphere i is measured.

The EM algorithm, proposed by Sidky [33], is a commonly used iterative approach to unfold the neutron spectrum. It has the advantages of less interference from noise, faster convergence, and better spectral solution, so it is widely used in industrial computed tomography and medical imaging. The iterative equation of the EM algorithm is [33]:

$$\Phi_j^{K+1} = \Phi_j^K \sum_i R_{ij}\left(\frac{N_i}{\sum_s R_{is}\Phi_s^K}\right) \tag{7}$$

2.3. The BSS system verification and experimental measurements

In order to obtain the neutron spectrum of the accelerator, it is necessary to carry out spectrum verification on the BSS system. The spectrum of the ^{241}Am–Be neutron source was measured at the Northwest Institute of Nuclear Technology. The ^{241}Am–Be neutron source is a cylindrical source with dimensions of 4 cm in height and 2 cm in diameter, and an activity of 2×10^5 n/s (measured in 2012). The layout of the experimental system is shown in Fig. 5.

The ^{241}Am–Be neutron source used in the experiment was housed in a cylindrical polyethylene shielding device with a diameter of 1.2 m, and the source was raised by a remote-control transmission device to irradiate the detector. The detector was placed 35 cm away from the transmission rod, and tested 10 times.

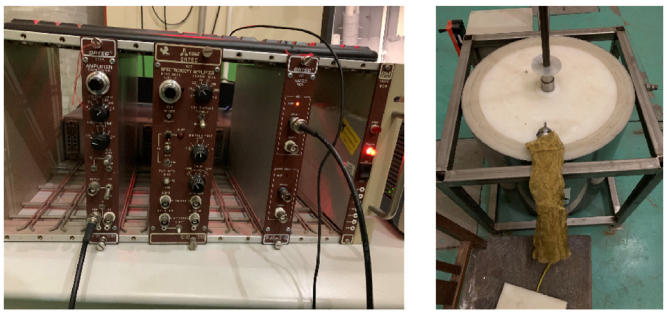

(a) (b)

Fig. 5. ^{241}Am–Be neutron source measurement layout.

The ^{241}Am–Be neutron spectrum was unfolded from the mean count rates of the spectrometer spheres, and it was compared with the standard ^{241}Am–Be spectrum provided by the International Organization for Standardization (ISO) [34]. As a result, the BSS system was used in this experiment to measure the neutron spectrum of the 120 MeV electron linac with power applied. This linac is from the Northwest Institute of Nuclear Technology [1]. The photocathode of the linac can produce electron beams of about 4–5 MeV into the accelerating tube, and one tube can accelerate electrons up to about 60 MeV.

The verified system was located 3.2 m from the first accelerating tube to measure the spectrum of the linac. The experimental layout is shown in Fig. 6.

As shown in the figure, the spectrum at the center of the first accelerating tube was measured by the BSS system. During the experiment, the first accelerating tube produced the most undesirable neutron, hence the neutron spectrum was measured using only the first accelerating tube. In this process, neutrons are mostly made by free electrons in the electron gun, free electrons in the accelerator tube, and X-rays made by electron bremsstrahlung. By applying various high voltages to the accelerating tube, it is found that when the tube is applied with 36.5 kV, the number of neutrons remained stable. Thus, the voltage of the accelerating tube is 36.5 kV in the experiment.

3. Results and discussion

3.1. The BSS energy response simulation and calibration

The MCNP Code was used to establish the same physical model as the actual detector. A series of simulation results for the BSS response are achieved as shown in Fig. 7.

As the thickness of the polyethylene spherical shell increases, the peak of the BSS neutron reaction shifts from the thermal neutron energy region to the high-energy neutron energy region. Furthermore, the energy response of the detector decreases rapidly

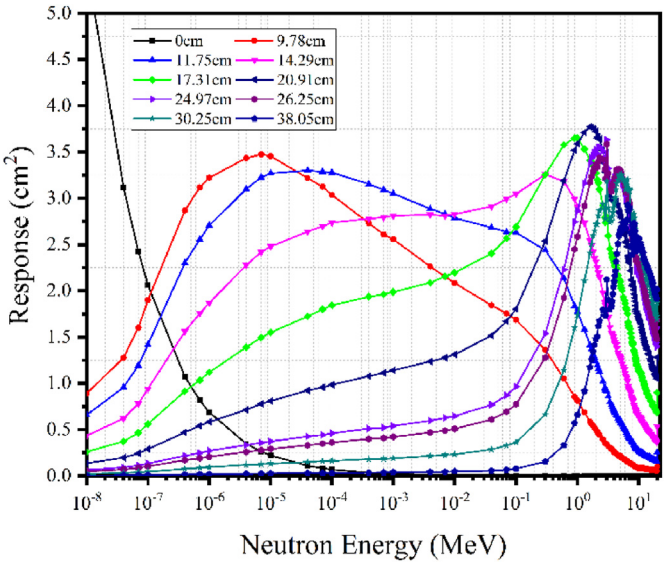

Fig. 7. BSS system energy response.

as the neutron energy exceeds 20 MeV, resulting in extremely low sensitivity for neutrons beyond 20 MeV.

The simulation results above were calibrated by using neutrons with energies of 2.86 MeV and 14.84 MeV produced by the Cockcroft-Walton accelerator. We calculated the detection response using Eqn. (1), and fit the detection efficiencies of these two energy points to the simulated detection response curves with a least-square fitting to obtain the calibration coefficients for spheres of different shell thicknesses. Eqn. (8) illustrates the least-square fitting:

$$L = \underset{a_1,a_2\ldots a_n}{argmin} \sum_{i=1}^{N} [f(x_i; a_1, a_2 \ldots a_n) - y_i]^2 \tag{8}$$

$f(x_i; a_1, a_2 \ldots a_n)$ in the formula is the response curve calculated by using the MCNP simulation, and y_i is the response of the spherical spectrometer at two neutron energies measured experimentally. By fitting the response curve calculated by simulation with the actual response value measured by experiment, the calibration coefficient between the simulated response and the actual response of each spectrometer can be obtained, so as to obtain the spherical spectrometer system under the condition of the all energy range real response.

The calibration coefficients obtained through the above process are shown in Table 2.

Since the true value of the measured data could not be obtained due to the influence of various factors during the experiment, uncertainty is used to describe its dispersion (see Table 3). The

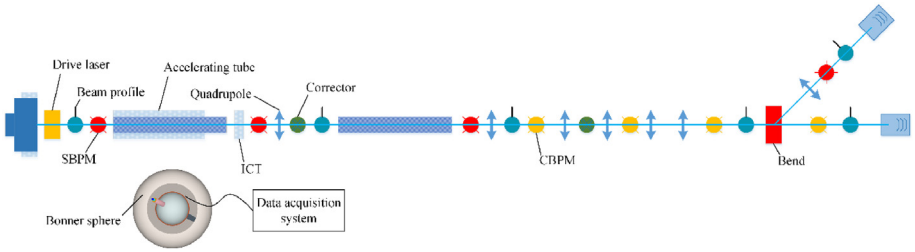

Fig. 6. Experimental layout.

Table 2
Least-squares fitting coefficient.

Diameter (cm)	0	9.78	11.75	14.29	17.31	20.91	24.97	26.25	30.25	38.05
Fitting coefficient	0.9023	1.438	1.419	1.308	1.211	1.134	1.089	0.9450	1.055	1.133

Table 3
Uncertainty of the calibration experimental process.

Sources of uncertainty	Type	Uncertainty/%
Neutron count rate	A	1
α count rate	A	2
BF_3 gas density	B	8
Density change of polyethylene spherical shell	B	7
Gamma-ray influence	B	0.5
Location influence	B	1
Neutron scattering	B	1
Total uncertainty		10.97

uncertainty of the calibration experiment mainly came from the detector counting and flux detection. The analysis of uncertainty gives the following table, which indicates that the total uncertainty is 10.97%.

3.2. Experimental results of the ^{241}Am–Be neutron source

The spectrum of the ^{241}Am–Be neutron source was measured by the calibrated BSS. Since the experimental hall was spacious and empty, the influence of neutron scattering could be neglected. Meanwhile, the detector presented very low sensitivity to gamma rays, which deposited little energy and were mainly concentrated in the low energy region of the counting spectrum. Therefore, by increasing the threshold, it is possible to remove the gamma ray count in the low energy region to obtain the neutron count spectrum. Table 4 summarizes the results of the measurement. The neutron spectrum of the ^{241}Am–Be source presented in Fig. 8 was obtained by feeding the measured count rate data into the precompiled Gravel and EM algorithms.

As shown in Fig. 8, after normalization, the spectrum unfolded by the Gravel algorithm is consistent with the spectrum of the ^{241}Am–Be neutron source provided by the ISO [34]. Several flux density peaks shown in the unfolded spectrum are generally in line with those in the ISO spectrum of the ^{241}Am–Be neutron source as well. On the other hand, the spectrum unfolded by the EM algorithm is consistent with the ISO spectrum from the perspective of peaks, while such two spectrums display different flux densities. At the same time, both algorithms have problems in that the flux density obtained by the solution is too high in the high energy section and the decrease is faster in the low energy section. It can also be seen from the figure that there are problems of oscillation and a high peak value in the spectrum solution results of the EM algorithm.

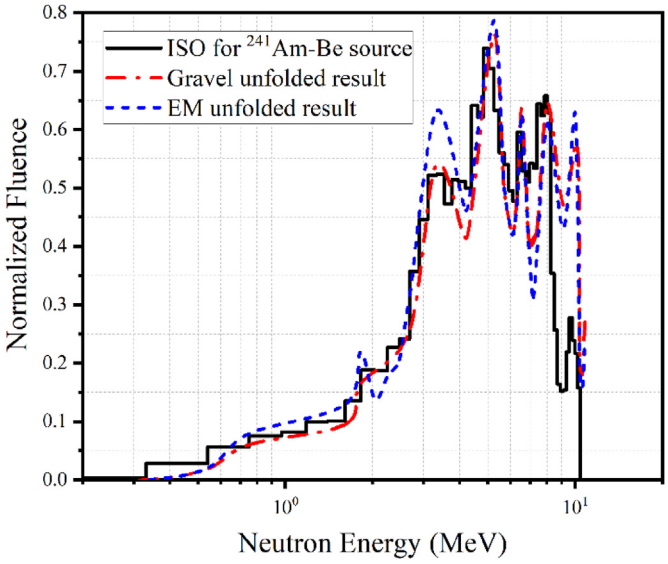

Fig. 8. Unfolded results of the ^{241}Am–Be neutron source.

The processes of detector calibration and simulation also influence the unfolding of the spectrum to some extent. As seen from the above analysis, the Gravel algorithm is effective in unfolding the spectrum of the ^{241}Am–Be neutron source, while the EM algorithm shows a mediocre effect in unfolding the multi-peak spectrum.

The uncertainty in the measurement results for the unfolding of the ^{241}Am–Be neutron source spectrum is shown in Table 5, which indicates a total uncertainty of less than 22% [35].

3.3. Experimental results of the spectrum of the linac neutron source

The reliability and accuracy of the BSS system was proven by calibrating the spectrum of the ^{241}Am–Be neutron source. Therefore, this system was utilized to measure the linac's neutron spectrum. The results are shown in Table 6.

According to the data shown in Table 6, the neutron spectrum at a distance of 3.2 m from the linac can be unfolded by Gravel and EM algorithms, with results shown in Fig. 9.

Fig. 9 illustrates the good conformity of spectrums unfolded by the Gravel and EM algorithms, which indicates that the majority of

Table 4
Experimental data of ^{241}Am–Be neutron source.

Diameter (cm)	Live time (s)	Total counts (10^4 counts)	Count rate (s^{-1})
0	52200	15.67	3.002
9.78	50400	60.53	12.01
11.75	72000	175.3	24.35
14.29	50400	151.7	30.10
17.31	3760	12.95	34.44
20.91	7200	26.04	36.16
24.97	6342	24.54	38.70
26.25	5351	20.55	38.40
30.25	10800	38.50	35.65
38.05	57600	168.4	29.23

Table 5
Uncertainty of the experimental process.

Sources of uncertainty	Type	Uncertainty/%
Detector energy response	A	10.97
Detector count rate	A	4
BF_3 gas density	B	8
Density change of polyethylene spherical shell	B	7
Gamma-ray influence	B	0.5
Location influence	B	2
Exposure time and decay effects	B	0.3
Source intensity	B	1.5
Unfolded process	B	15
Total uncertainty		21.93

Table 6
Experimental results of linac undesirable neutrons.

Diameter (cm)	Live time (s)	Total counts (10^4 counts)	Count rate (s^{-1})
0	64800	3.765	0.5810
9.78	115200	20.42	1.172
11.75	54000	13.15	2.436
14.29	64800	15.95	2.462
17.31	31200	9.849	3.157
20.91	40359	10.95	2.713
24.97	43200	7.917	1.832
26.25	39600	6.739	1.702
30.25	28743	2.982	1.038
38.05	32400	2.067	0.6381

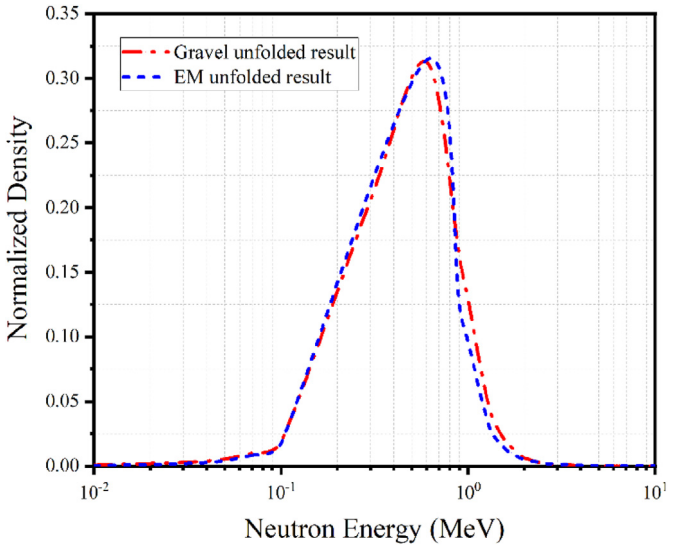

Fig. 9. Neutron spectrum of linac.

the neutrons produced by the accelerator are concentrated between 0.1 and 2 MeV for the single peak. It is worth mentioning that the 9.78 cm Bonner sphere presents a broad detection response curve and lower energy resolution during the unfolding process, so it is necessary to subtract it during the unfolding process to produce a more accurate spectrum.

To determine the neutron dose equivalent at the measurement point, we referred to the International Commission on Radiological Protection (ICRP) [36] flux-dose conversion coefficient, which can be calculated by the following equation:

$$H_{p,slab}(10,0^\circ) = \sum_{i=1}^{n} \frac{\Phi_1(E_i)}{\Phi(E_i)} h_{p,slab}(10,0^\circ) \quad (9)$$

The undesirable neutron dose equivalent at a distance of 3.2 m from the linac, calculated by using Eqn. (9), is 1.978 × 10^{-2} mSv/h.

Table 7
Uncertainty of the experimental process.

Sources of uncertainty	Type	Uncertainty/%
Detector energy response	A	10.97
Recording time	A	7
BF_3 gas density	B	8
Density change of polyethylene spherical shell	B	7
Gamma-ray influence	B	0.5
Location influence	B	1
Unfolded process	B	15
Total uncertainty		22.55

The uncertainty of the experimental process is summarized in Table 7, and the total uncertainty is less than 23%.

3.4. Discussion

To obtain the neutron spectrum in the linac hall, we set up a spectrometer system consisting of 10 Bonner spheres with different diameters and a proportional counter tube. The response of each sphere was simulated using MCNP, and calibration experiments were performed on a Cockcroft-Walton accelerator using neutrons at 2.86 MeV and 14.84 MeV. Then we used the calibrated spectrometer system to measure the spectrum of the ^{241}Am–Be neutron source. During the experiment, each spherical spectrometer was equipped with a proportional counter tube for a single measurement, and the measurement position was consistent for each measurement. During the experiment, it was ensured that the peak counts recorded by the software exceeded 10^3 to reduce the impact of statistical fluctuations. By comparing the spectral analysis results with the standard spectrum of the ^{241}Am–Be neutron source given by ISO, the results showed that the spectrometer system has high reliability in measuring the neutron spectrum. Finally, we measured the neutron spectrum in the linac hall, and obtained the spectrum and dose equivalent of 1.978 × 10-2 mSv/h at a distance of 3.2 m from the accelerating tube while keeping the statistical fluctuation low.

4. Conclusions

The measurement of the undesirable neutron spectrum of linac has always been a preoccupation of researchers. To obtain the undesirable neutron spectrum of the linac and to quantitatively study the photoneutron impacts during the experiment, we used existing equipment to construct a BSS system based on BF_3 gas proportional counter tubes. The actual energy response of the BSS system was obtained through simulation and calibration experiments. The spectrum of the ^{241}Am–Be neutron source was then measured to verify that the measurement results of the BSS system were reliable under the unfolding algorithms and were in good compliance with the standard spectrum. Finally, the undesirable neutron spectrum of the linac was measured using the verified BSS system to obtain the spectrum at a distance of 3.2 m from the accelerator and the neutron dose equivalent.

It can be concluded that the entire measurement system for the fast neutron spectrum developed in this paper can measure the spectrum in the accelerator neutron field accurately; therefore, it can be used to measure the fast neutron spectrum in environments with low neutron yield, thus to laying solid foundation for future neutron flux measurement and dose detection.

CRediT authorship contribution statement

Yihong Yan: Conceptualization, Methodology, Software, Data curation, Writing-original draft, Writing - review & editing. **Xinjian Tan:** Conceptualization, Methodology, Software. **Xiufeng Weng:** Data curation, Formal analysis. **Xiaodong Zhang:** Data curation, Data analysis. **Zhikai Zhang:** Software, Data curation, Writing - review. **Weiqiang Sun:** Software, Data curation. **Guang Hu:** Writing - review & editing. **Huasi Hu:** Writing - review & editing, Investigation.

Declaration of competing interest

The authors declare that they have no known competing financial interests or personal relationships that could have appeared to influence the work reported in this paper.

Acknowledgement

This work is supported by the NSAF Joint Fund set up by the National Natural Science Foundation of China and the Chinese Academy of Engineering Physics under Grant (U1830128); the Foundation of Key Laboratory of Nuclear Reactor System Design Technology, Chinese Academy of Nuclear Power; and the National Natural Science Foundation of China (No. 11975182).

References

[1] B. Sun, Y. Wang, D.W. Hei, et al., Development of online automatic conditioning system in electron linear accelerator[J], Atomic Energy Sci. Technol. 8 (2019) 1517–1522.
[2] Y. Yu, X. Weng, Y. Yang, et al., The study of fast neutrons production via the electrodisintegration reactions of high energy electrons[J], Nucl. Instrum. Methods Phys. Res. 954 (2020) 161747–161751.
[3] Q. Wang, X. Weng, Y. Yu, et al., Investigation of fast neutron resonance transmission analysis based on the ultrashort pulsed electron beam-driven photoneutron source[J], J. Instrum. 14 (5) (2019). P05004-P05004.
[4] X. Chen, Z.C. Zhang, K. Zhang, et al., Study on the time response of a barium fluoride scintillation detector for fast pulse radiation detection[J], IEEE Trans. Nucl. Sci. (99) (2020), 1-1.
[5] M.J. Gadlage, A.H. Roach, A.R. Duncan, et al., Soft errors induced by high-energy electrons[J], IEEE Trans. Device Mater. Reliab. 17 (1) (2017) 157–162.
[6] M.J. Gadlage, A.H. Roach, A.R. Duncan, et al., Multiple-cell upsets induced by single high- energy electrons[J], IEEE Trans. Nucl. Sci. 65 (1) (2018) 211–216.
[7] T.G. Soto-Bernal, A. Baltazar-Raigosa, D. Medina-Castro, et al., Neutron production during the interaction of monoenergetic electrons with a Tungsten foil in the radiotherapeutic energy range[J], Nucl. Instrum. Methods Phys. Res. (2017) 27–38.
[8] T.G. Soto-Bernal, A. Baltazar-Raigosa, D. Medina-Castro, et al., Neutron production in the interaction of 12 and 18MeV electrons with a scattering foil inside a simple LINAC head, [J]. Appl Radiat Isot (2018) 46–52.
[9] M. Stefanik, P. Bem, M. Majerle, et al., Neutron Spectrum Determination of d(20)+Be Source Reaction by the Dosimetry Foils method[J], Radiation Physics & Chemistry, 2017. S0969806X17303225.
[10] M. tefánik a b, P. Bém a, A.M. G, et al., Neutron spectrum determination of the p(35 MeV)-Be source reaction by the dosimetry foils method[J], Nucl. Data Sheets 119 (1) (2014) 422–424.
[11] H.J. Kim, I.S. Hahn, M.J. Hwang, et al., Measurement of the neutron flux in the CPL underground laboratory and simulation studies of neutron shielding for WIMP searches[J], Astropart. Phys. 20 (5) (2004) 549–557.
[12] V. Chazal, R. Brissot, J.F. Cavaignac, et al., Neutron background measurements in the underground laboratory of Modane[J], Astropart. Phys. 9 (2) (1997) 163–172.
[13] H.R. Vega-Carrillo, A.E. Manzanares-Acuña, Background neutron spectrum at 2420 m above sea level[J], Nucl. Instrum. Methods Phys. Res. 524 (1–3) (2004) 146–151.
[14] A. Esposito, R. Bedogni, C. Domingo, et al., Measurements of leakage neutron spectra from a high-energy accumulation ring using Extended Range Bonner Sphere Spectrometers[J], Radiat. Meas. 45 (10) (2010) 1522–1525.
[15] R. P, Belli, et al., Deep Underground Neutron Flux Measurement with Large BF_3 counters[J], IL Nuovo Cimento A, 1989.
[16] P. Goldhagen, M. Reginatto, T. Kniss, et al., Measurement of the energy spectrum of cosmic-ray induced neutrons aboard an ER-2 high-altitude airplane[J], Nuclear Instruments and Methods in Physics Research Section A Accelerators Spectrometers Detectors and Associated Equipment 476 (1–2) (2002) 42–51.
[17] B. Wiegel, S. Agosteo, R. Bedogni, et al., Intercomparison of radiation protection devices in a high-energy stray neutron field, Part II: Bonner sphere spectrometry[J], Radiat. Meas. 44 (7) (2009).
[18] A. Baltazar-Raigosa, H.R. Vega-Carrillo, A. Garcia-Duran, et al., Novel passive nested bonner cubes spectrometer for neutrons and its response matrix[J], The European Physical Journal Plus 136 (10) (2021) 1–13.
[19] S.J. Boot, J.A.B. Gibson, A Counter for Measuring Neutron Dose Equivalent from Thermal Energies to 10 keV[R]. Harwell, UKAEA/Atomic Energy Research Establishment, 1978. Report AERER-9357.
[20] B. Burgkhardt, G. Fieg, A. Klett, et al., The neutron fluence and H*(10) response of the new LB 6411 REM counter[J], Radiat. Protect. Dosim. 70 (1) (1997) 361–364.
[21] C. Birattari, A. Ferrari, C. Nuccetelli, et al., An extended range neutron rem counter[J], Nucl. Instrum. Methods Phys. Res., Sect. A 297 (1–2) (1990) 250–257.
[22] M. Mourgues, J.C. Carossi, G. Portal, A Light Rem-Counter of Advanced technology[C]. Neutron Dosimetry, Proc. Eurtom 5th Symp. Neuherberg, 1984.
[23] D.T. Bartlett, R.J. Tanner, D.G. Jones, A new Design of neutron dose equivalent survey instrument[J], Radiat. Protect. Dosim. 74 (4) (1997) 267–271.
[24] V. Mares, G. Schraube, H. Schraube, Calculated neutron response of a Bonner sphere spectrometer with 3He counter[J], Nucl. Instrum. Methods Phys. Res. 307 (2–3) (1991) 398–412.
[25] V. Mares, H. Schraube, Evaluation of the response matrix of a Bonner sphere spectrometer with LiI detector from thermal energy to 100 MeV[J], Nucl. Instrum. Methods Phys. Res. 337 (2–3) (1994) 461–473.
[26] A. Aroua, M. Grecescu, P. Lerch, et al., Evaluation and test of the response matrix of a multisphere neutron spectrometer in a wide energy range Part I. Calibration[J], Nucl. Instrum. Methods Phys. Res. 321 (1–2) (1992) 298–304.
[27] T.E. Booth, S. Avneet, T.J. Goorley, S. Jeffrey, B.F. Brown, R. Arthure, MCNP—A General Monte Carlo N-Particle Transport Code, Version 5: LA-UR-03-1987, Los Alamos National Laboratory, Los Alamos, NM, USA, 2003.
[28] Evaluated Nuclear Data File, ENDF/B-VIII.0 released, Available online: https://www.nndc.bnl.gov/exfor/endf00.jsp, February 2, 2018. (Accessed 25 February 2022).
[29] J.M. Gomez-ros, R. Bedogni, D. Bortot, et al., CYSP: a new cylindrical directional neutron spectrometer, Conceptual design[J]. Radiation measurements (2015) 8247–8251, https://doi.org/10.1016/j.radmeas.2015.07.005.
[30] W. Rühm, V. Mares, C. Pioch, et al., Comparison of Bonner sphere responses calculated by different Monte Carlo codes at energies between 1MeV and 1GeV – potential impact on neutron dosimetry at energies higher than 20 MeV[J], Radiat. Meas. 67 (2014) 24–34.
[31] M. Matzke, Unfolding of Pulse Height Spectra: the HEPRO Program system[R], PTB-Report PTB-N-19, PTB Braunschweig, 1994.
[32] Matzke Manfred, Unfolding of Particle spectra[J], Physikalisch-Technische Bundesanstalt (Germany), 1997, p. 2867.
[33] E.Y. Sidky, L.F. Yu, X.C. Pan, et al., A robust method of X-ray source spectrum estimation from transmission measurements: demonstrated on computer-simulated, scatter-free transmission data[J], J. Appl. Phys. 97 (12) (2005) 1–11.
[34] International Organization for Standardization, Reference Neutron Radiations-Part I: Characteristics and Methods of Production, 2000. ISO 8529-1.
[35] S.J. Chen, et al., Measurement uncertainty and its estimation[J], The Administration And Technique Of Environmental Monitoring 14 (5) (2002) 38–43.
[36] ICRP, ICRP publication 74: conversion coefficients for use in radiological protection against external radiation[J], Annals of the Icrp 26 (1997).